Optical absorption in $Hg_{1-x}Cd_xSe$ alloys

C. J. Summers and J. G. Broerman
McDonnell-Douglas Research Laboratories, McDonnell-Douglas Corporation, St. Louis, Missouri 63166
(Received 3 August 1979)

Infrared transmission measurements between 1 and 25 μm are reported for $Hg_{1-x}Cd_xSe$ alloys with $0.15 < x < 0.68$ and electron concentrations between 1×10^{16} and 9×10^{16} cm^{-3} at temperatures between 5 and 300 K. The data have been analyzed to obtain the refractive index and the intrinsic-absorption-coefficient spectrum for each sample and sample temperature. From fits of these data using an optical-absorption theory based on the Kane three-band model, accurate values for the fundamental energy-gap and conduction-band parameters were obtained. Empirical relationships are reported for the dependences of the refractive index, fundamental energy gap, and energy-band parameters on alloy composition and temperature. For temperatures between 5 and 300 K the refractive index decreases with increasing x values and at 5 K has values of 3.92 and 2.68 for x values of 0.153 and 0.684, respectively. For the same temperature and range of alloy compositions, the energy gap increases from 0.031 to 1.029 eV. The dependence of the energy gap on alloy composition bows slightly below a linear interpolation between the energy gaps of HgSe and CdSe. Like other II-VI and IV-VI ternary alloy systems, low-x $Hg_{1-x}Cd_xSe$ alloys exhibit large, positive, energy-gap temperature coefficients.

I. INTRODUCTION

Historically, optical measurements have long been used to investigate the properties of solids. This is particularly true of semiconducting materials, where measurements of optical-transmittance spectra enable the energy gap and refractive index to be determined for a wide range of temperatures in both large and small band-gap semiconductors. Such studies were first used to measure the properties of elemental and binary semiconductors, and more recently, ternary and quaternary systems. Recently, improved methods of crystal growth for alloys of mercury cadmium selenide have produced ingots of sufficient crystalline perfection and homogeneity to permit a detailed study of this alloy system.[1] In this paper a precise determination of the dependence of the fundamental energy gap and other energy-band parameters on crystal composition and temperature is reported for $Hg_{1-x}Cd_xSe$ alloys with $0.15 \leq x \leq 0.68$, where x is the mole fraction of CdSe. These material constants describe the fundamental properties of a semiconductor alloy system and are required to calculate the intrinsic limits of technologically important properties, such as the electron concentration, mobility, and lifetime, as functions of alloy composition and temperature.

The properties of the two end components of the HgSe-CdSe system are reasonably well known. Magnetoresistence and galvanomagnetic measurements have shown that HgSe is a perfect (symmetry-induced) semimetal,[2] and results of these studies have been analyzed to determine the value of the energy gap at the center of the Brillouin zone.[3,4] The Γ_6-Γ_8 energy gap is strongly dependent on temperature,[4] varying from −0.22 eV at 5 K to −0.06 eV at 300 K. Optical studies[5,6] show that CdSe has the conventional band structure for a II-VI compound with the conduction and valence-band extrema both occurring at $k = 0$, separated by an energy gap of 1.84 eV at 5 K and ~1.7 eV at 300 K.

Using sintered samples, Kalb and Leute[7] showed that $Hg_{1-x}Cd_xSe$ alloys with $0 < x < 0.77$ have the zinc-blende structure and form an almost perfect range of solid solutions in which the lattice mismatch is less than 0.03%. Alloys with $x > 0.81$ were found to have the wurtzite structure, proving that the miscibility gap between the two solid phases is small.

Previous electrical[8] and optical[9,10] investigations of alloys with the zinc-blende structure show that, with increasing x, a smooth transition occurs from the semimetallic properties of HgSe to the semiconducting behavior typical of a direct-band-gap zinc-blende semiconductor. Measurements of the fundamental absorption spectrum have been reported by Kireev and Volkov[9] for thin-film $Hg_{1-x}Cd_xSe$ samples with x values between 0.1 and 0.6 and by Slodowy and Giriat[10] at 100 K and 295 K for Bridgman-grown samples with x values between 0.2 and 0.6. However, no attempt was made in either investigation to analyze the data to obtain precise values for the fundamental energy gap.

Experimental investigations of many mixed-

crystal III-V and II-VI systems[11] have established that in all these systems, the variation of the fundamental energy gap E_G, with crystal composition is sublinear and described by the equation

$$E_G = a + bx + cx^2 , \quad (1)$$

where c, the bowing parameter, is positive and measures the departure from linear behavior. It is assumed that the $Hg_{1-x}Cd_xSe$ system behaves in a similar manner and that the properties of zinc-blende-structured $Hg_{1-x}Cd_xSe$ alloys with positive energy gaps are described by the band structure first proposed by Kane[12] for InSb. In this model the smallest energy difference occurs at $k=0$ between the $s^{1/2}$-like Γ_6 level and the $p^{3/2}$-like Γ_8 level (Fig. 1). Alloys with the wurtzite structure are described by a similar band structure in which the degeneracy of the light-hole and heavy-hole valence bands at $k=0$ is broken by the lower crystal-field symmetry producing a small (≈ 0.02 eV) splitting[5] between the two valence bands. Material parameters required for CdSe crystals with the zinc-blende-structure are therefore expected to be closely approximated by averaging the values reported for CdSe crystals with the wurtzite structure.

At present there is no complete theoretical description of either the compositional or temperature dependence of the energy gap and no unified theory that explicitly calculates the effect of these dependences on energy-band shapes in pseudobinary alloy semiconductors. The compositional effect has been shown to be significant,[13,14] and in 1957 Ehrenreich[15] suggested that the temperature dependence of the conduction-band shape can be calculated empirically using an effective energy gap in Kane's theory. The effective energy gap includes only the effect of lattice dilation with temperature, whereas the experimentally measured energy gap is affected by both lattice dilation and electron-photon coupling. In low-x $Hg_{1-x}Cd_xSe$ samples, a large temperature dependence of the energy gap is observed and attributed primarily to electron-phonon coupling. Because of the magnitude of this mechanism, the effective energy-gap model suggested by Ehrenreich was not used, and the optical absorption spectra obtained in this study were analyzed using Kane's energy band model despite the fact that this theory is strictly valid only at absolute zero. Because extrinsic and thermally excited electrons prevent accurate values of the fundamental band-gap energy from being obtained directly from the experimental data, a theoretical treatment of the absorption coefficient was formulated that accurately considers the temperature dependence of the electron population, the nonparabolicity of the band structure, and the energy dependence of the optical transition probability. By fitting the calculated absorption coefficients to the experimental data, the Kane energy-band parameters were determined, and their dependence on alloy composition and temperature were obtained. The details of this calculation are given in the following section of this paper.

II. THEORY

The energy-band model used for calculating the theoretical absorption coefficient is shown in Fig. 1. The contribution to the absorption coefficient of optical transitions from the heavy-hole and light-hole valence bands to the conduction band are computed considering the dependence of the optical transition strength on photon energy. Attention is given to the presence of thermally excited or impurity-generated conduction electrons, which produce a Moss-Burstein shift for optical transitions between the valence and conduction bands and at finite temperatures modify the strength of the absorption coefficient for energies $\approx 2k_BT$ above or below the Fermi energy, where k_B is Boltzmann's constant and T is the absolute temperature.

The fundamental quantity from which all optical properties can be calculated is the complex dielectric constant. This is calculated in the

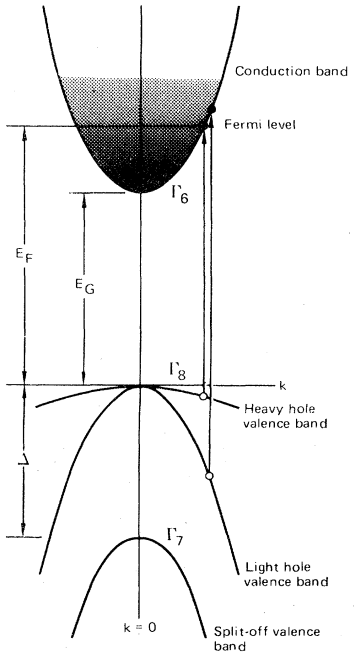

FIG. 1. Energy level structure and transitions used for the calculation of the optical absorption coefficient

random-phase approximation[16] and expressed in terms of the fundamental energy gap, conduction-band–valence-band momentum matrix element, and spin-orbit splitting. The complex dielectric function $\epsilon(\omega)$ can be expressed as the sum of a lattice part, an interband electronic part, and an intraband electronic part:

$$\epsilon(\omega)=\epsilon(\omega)^{\text{lat}}+\epsilon(\omega)^{\text{inter}}+\epsilon(\omega)^{\text{intra}} \tag{2}$$

The interband electronic contribution is given by the relation

$$\epsilon(\omega)^{\text{inter}}=-\lim_{q\to 0}\frac{e^2}{\pi^2 q^2}\times\sum_{\substack{i,j\\ i\neq j}}\int d^3k\frac{|\langle i,\vec{k}|e^{-i\vec{q}\cdot\vec{r}}|j,\vec{k}+\vec{q}\rangle|^2}{E_{\vec{k}+\vec{q},j}-E_{\vec{k},i}-\hbar\omega-i\hbar/\tau_{ij}}\times[f(E_{\vec{k}+\vec{q},j})-f(E_{\vec{k},i})]\,, \tag{3}$$

where the τ_{ij} are lifetimes associated with $i\neq j$ excitations, $E_{\vec{k},i}$ is the energy of the ith band at crystal momentum $\vec{k}$, $f(E_{\vec{k},i})$ is the Fermi distribution function, ω is the angular frequency, and $\vec{q}$ is the momentum transfer. The interband contribution to the dielectric constant can be further divided into three parts: a light-hole–conduction-band excitation, a heavy-hole–conduction-band excitation, and a background from all other higher-energy excitations ϵ_b:

$$\epsilon(\omega)^{\text{inter}}=\epsilon(\omega)^{lh\text{-}c}+\epsilon(\omega)^{hh\text{-}c}+\epsilon_b\,. \tag{4}$$

Because of the large energy differences between the states contributing to the background, ϵ_b is real and has no frequency dependence in the infrared. Values for $\epsilon(\omega)^{lh\text{-}c}$ and $\epsilon(\omega)^{hh\text{-}c}$ are calculated for the Kane three-band model,[12] which considers the $\vec{k}\cdot\vec{p}$ interactions between the Γ_6 conduction band, the Γ_8 light-hole band, and the Γ_7 split-off valence band. The heavy-hole band is considered to be parabolic and is characterized by an effective mass μ_{hh}, i.e.,

$$E_{\vec{k},hh}=-\hbar^2k^2/2\mu_{hh}m_0\,, \tag{5}$$

where m_0 is the free-electron mass. The energies of the conduction, light-hole, and split-off bands are given by the solutions of the secular equation

$$E(E-E_G)(E+\Delta)-k^2P^2(E+2\Delta/3)=0\,, \tag{6}$$

where P is the momentum-matrix element, Δ is the valence-band spin-orbit splitting, E_G is the fundamental gap, and the free-electron energy $(\hbar^2k^2/2m_0)$ is assumed to be negligible. The light-hole–conduction-band and heavy-hole–conduction-band matrix elements are then calculated to second order in q to be

$$|\langle lh,\vec{k}|e^{-i\vec{q}\cdot\vec{r}}|c,\vec{k}+\vec{q}\rangle|^2=\frac{L_2^{lh\text{-}c}}{k}q^2\cos^2\theta-\frac{L_0^{lh\text{-}c}}{k^2}q^2\sin^2\theta \tag{7}$$

and

$$|\langle c,\vec{k}|e^{-i\vec{q}\cdot\vec{r}}|hh,\vec{k}+\vec{q}\rangle|^2=\frac{(b_c+\sqrt{2}\,c_c)^2}{4}\frac{q^2\sin^2\theta}{k^2}. \tag{8}$$

In Eqs. (7) and (8), θ is the angle between $\vec{k}$ and $\vec{q}$, and the functions $L_2^{lh\text{-}c}$, $L_0^{lh\text{-}c}$, b_c, and c_c, are defined in Appendix A. Taking the limit as $q\to 0$ and evaluating the angular integrations, one obtains

$$\epsilon(\omega)^{lh\text{-}c}=\frac{4e^2}{3\pi}\int_0^{k_{\text{BC}}}dk\left[[f(E_{k,lh})-f(E_{k,c})][(kL_0^{lh\text{-}c})]\times\left(\frac{1}{E_{k,c}-E_{k,lh}-\hbar\omega-i\hbar/\tau_{c,lh}}+\frac{1}{E_{k,c}-E_{k,lh}+\hbar\omega+i\hbar/\tau_{c,lh}}\right)\right] \tag{9}$$

and

$$\epsilon(\omega)^{hh\text{-}c}=\frac{2e^2}{3\pi P}\int_{E_G}^{E_{\text{BC}}}dE\,G(E)[f(E_{hh})-f(E)]\left(\frac{1}{E-E_{hh}-\hbar\omega-i\hbar/\tau_{c,hh}}+\frac{1}{E-E_{hh}+\hbar\omega+i\hbar/\tau_{e,hh}}\right), \tag{10}$$

where

$$G(E)=\frac{[2E^3+(3\Delta-E_G)E^2+(4\Delta/3)(\Delta-E_G)E-2\Delta^2E_G/3](E-E_G)^{1/2}(E+\Delta)^{3/2}}{E^{1/2}(E+2\Delta/3)^{3/2}[N_c(E)]^2}, \tag{11}$$

$$E_{hh}=-\frac{\hbar^2}{2\mu_{hh}m_0}\frac{E(E-E_G)(E+\Delta)}{P^2(E+2\Delta/3)}, \tag{12}$$

k_{BC} and E_{BC} are, respectively, the crystal momentum and conduction-band energy at the edge of the Brillouin zone, and $N_c(E)$ is defined in Appendix A.

The intraband electronic contribution to the complex dielectric constant,

$$\epsilon(\omega)^{\text{intra}} = -\lim_{q\to 0}\frac{e^2}{\pi^2 q^2}\sum_{i=c,lh,hh}\int d^3k\,\frac{|\langle i,\vec{k}|\,e^{-i\vec{q}\cdot\vec{r}}\,|i,\vec{k}+\vec{q}\rangle|^2}{E_{\vec{k}+\vec{q},i}-E_{\vec{k},i}-\hbar\omega-i\hbar/\tau_i}[f(E_{\vec{k}+\vec{q},i})-f(E_{\vec{k},i})], \tag{13}$$

is similarly calculated. The following results are obtained for the electron (ϵ^c), light-hole (ϵ^{lh}), and heavy-hole (ϵ^{hh}) contributions:

$$\epsilon^c(\omega) = -\frac{1}{(\omega+i/\tau_c)^2}\frac{8e^2}{3\pi P\hbar^2 k_B T}\int_{E_G}^{E_{BC}} dE\,\frac{[E(E-E_G)(E+\Delta)]^{3/2}(E+2\Delta/3)^{1/2}}{[2E^3+(3\Delta-E_G)E^2+\frac{4}{3}\Delta(\Delta-E_G)E-\frac{2}{3}\Delta^2E_G]} \times\frac{\exp[(E-E_F)/k_BT]}{\{\exp[(E-E_F)/k_BT]+1\}^2}, \tag{14}$$

$$\epsilon^{lh}(\omega) = -\frac{1}{(\omega+i/\tau_{lh})^2}\frac{8e^2}{3\pi P\hbar^2 k_B T}\int_0^{-E_{Blh}} dE\,\frac{[E(E+E_G)(E-\Delta)]^{3/2}(E-2\Delta/3)^{1/2}}{[2E^3-(3\Delta-E_G)E^2+\frac{4}{3}\Delta(\Delta-E_G)E+\frac{2}{3}\Delta^2E_G]} \times\frac{\exp[(E+E_F)/k_BT]}{\{\exp[(E+E_F)/k_BT]+1\}^2}, \tag{15}$$

and

$$\epsilon^{hh}(\omega) = \frac{-4\pi N_{hh}e^2}{\mu_{hh}m_0(\omega+i/\tau_{hh})^2}, \tag{16}$$

where E_F is the Fermi energy, N_{hh} is the density of heavy holes, and E_{Blh} is the energy of the light-hole band at the edge of the Brillouin zone.

To evaluate these expressions for the electronic part of the dielectric function, values for the Fermi energy are required. These are found by solving numerically the charge neutrality condition,

$$N - N_{lh} - N_{hh} = N_D, \tag{17}$$

where N, N_{lh}, N_{hh}, and N_D are, respectively, the densities of electrons, light holes, heavy holes, and ionized donors. The following expressions for the charge-carrier densities are obtained from the secular equations:

$$N = \frac{1}{2\pi^2P^3}\int_{E_G}^{E_{BC}} dE\,f(E,Z)\frac{[2E^3+(3\Delta-E_G)E^2+(4\Delta/3)(\Delta-E_G)E-2\Delta^2E_G/3][E(E-E_G)(E+\Delta)]^{1/2}}{(E+2\Delta/3)^{5/2}}, \tag{18}$$

$$N_{lh} = \frac{1}{2\pi^2P^3}\int_0^{-E_{Blh}} dE\,f(E,-Z)\frac{[2E^3-(3\Delta-E_G)E^2+(4\Delta/3)(\Delta-E_G)E+2\Delta^2E_G/3][E(E+E_G)(E-\Delta)]^{1/2}}{(E-2\Delta/3)^{5/2}}, \tag{19}$$

and

$$N_{hh} = \frac{1}{2\pi^2}\left(\frac{2\mu_{hh}m_0k_BT}{\hbar^2}\right)^{3/2}F_{1/2}(-Z), \tag{20}$$

where

$$f(E,Z) = \frac{1}{\exp[(E/k_BT-Z)]+1}, \tag{21}$$

$$Z = E_F/k_BT, \tag{22}$$

and $F_{1/2}(Z)$ is the Fermi function of order $\frac{1}{2}$.

To calculate the observable optical properties, the total dielectric function is divided into its real and imaginary parts,

$$\epsilon = \epsilon_1 + i\epsilon_2, \tag{23}$$

and from these quantities the real and imaginary parts of the index of refraction, n^* and k^*, respectively, are calculated:

$$n^* = \frac{[\epsilon_1+(\epsilon_1^2+\epsilon_2^2)^{1/2}]^{1/2}}{\sqrt{2}} \tag{24}$$

and

$$k^* = \frac{\epsilon_2}{2n^*}. \tag{25}$$

The absorptance α and the single-surface reflectance R are then given by

$$\alpha = 4\pi k^*/\lambda \tag{26}$$

and

$$R = \frac{(n^*-1)^2+(k^*)^2}{(n^*+1)^2+(k^*)^2}. \tag{27}$$

The expression for α, Eq. (26), depends explicitly on the energy-band parameters and the Fermi energy, which is calculated from the measured electron concentration and the same set of energy-band parameters that are used later to calculate the theoretical absorption-coefficient-energy spectrum. By varying the band parameters used in this calculation, a best fit to the experimental absorption spectrum can be obtained for each sample at each temperature.

III. EXPERIMENTAL PROCEDURE

The single-crystalline ingots required for this comprehensive study were grown by the slow-growth Bridgman method from stoichiometric $Hg_{1-x}Cd_xSe$ melts with x values between 0.16 and 0.40. This growth procedure produced ingots with longitudinal compositional gradients in which compositions between ≈ 0.7 and 0.1 were obtained, depending on the initial melt composition and the growth conditions.[1] X-ray diffraction measurements confirmed that the samples used in this study had the zinc-blende structure and were free of inclusions containing the wurtzite phase.

A. Sample preparation

For this study, slices approximately 1 mm thick were cut from the ingots, etched in a 5% bromine-methanol solution, and annealed in vacuum between 473 and 523 K for periods up to 200 h. This heat treatment improved the uniformity of the material and reduced the extrinsic electron concentration by an order of magnitude to $1-5\times10^{16}$ cm^{-3}. The compositional homogeneity of each slice was assessed by an infrared scanning method in which the absorption edge was measured through a 1-mm diameter aperture which was scanned across the slice. Regions that were estimated to be homogeneous to within ±0.002 mole fraction CdSe were then cut from each slice, and their compositions were determined by mass-density measurements[17] with a precision $< \pm0.003$ mole fraction CdSe. The electron concentration and mobility from 4.2 to 300 K were measured for each pared sample using the van der Pauw method.[18] Compositionally homogeneous samples with normal electrical properties were further reduced in thickness for the optical-transmission measurements. Because some samples were cut from sections of Bridgman ingots that had a longitudinal compositional gradient, equal amount of material were removed from each surface to retain, as far as possible, the integrity of the compositional measurements. The final grinding and polishing were carefully performed to avoid surface damage,[19] which can have a significant effect on the shape of the optical-transmission edge, particularly at absorption-coefficient values below 100 cm^{-1}. For this step the specimens were bonded to a polishing holder with a low-melting-temperature (< 333 K) thermoplastic cement, and grinding and polishing were performed with successively finer abrasive grits. The layer thickness removed at each step was 4–10 times the diameter of the abrasive grit used in the preceding step, and the final-step grit was 0.03-μm diameter alumina powder. The optical absorption measurements and the x-ray topographic studies performed on these samples indicated that the surface damage was small. The thicknesses of the optical-absorption samples were between 10 and 100 μm and were measured with an accuracy of $\pm3\%$ with a calibrated electronic thickness gauge after the transmission spectra were recorded.

B. Optical measurements

Optical transmission spectra were recorded for wave numbers between 5000 and 400 cm^{-1} (2–25 μm) at a resolution of 2 cm^{-1} (0.00025 eV) with a Fourier-transform interferometer-spectrometer. The samples were mounted in a strain-free manner in an optical Dewar and cooled by a stream of He gas. The power to heaters placed in the He-gas stream was regulated to maintain sample temperatures stable to ±0.1 K for temperatures between 5–50 K and to ±0.2 K for temperatures between 50–300 K. The sample chamber was fitted with silicon windows, which were also cooled by the He-gas stream, and cesium iodide was used as a room-temperature window.

The absorption coefficient α was obtained from the expression

$$\mathcal{T}=\frac{(1-R)^2e^{-\alpha d}}{1-R^2e^{-2\alpha d}}, \tag{28}$$

where $\mathcal{T}$ is the transmittance of the sample, d is the sample thickness and R represents the single-surface reflection loss. R is calculated from the expression

$$R=\left(\frac{n^*-1}{n^*+1}\right)^2, \tag{29}$$

where n^* is the refractive index. The refractive index was calculated from the spectral data recorded at wavelengths longer than the transmission edge, either from the fringe spacing that was observed for most samples or from the maximum transmittance, which was assumed to occur at a wavelength where the absorption from both interband transitions and free electrons is negligible. The refractive index was calculated from

the fringe spacing according to the relation

$$n^* = \frac{m}{2d}\frac{1}{\nu_{n+m} - \nu_n}, \tag{30}$$

where ν_n and ν_{n+m} are the wave numbers at the nth and $(n+m)$th interference peaks, and m is the number of fringes between the peaks. When $\alpha = 0$, Eq. (28) reduces to

$$R = \frac{1-\mathcal{T}}{1+\mathcal{T}}. \tag{31}$$

If Eqs. (29) and (31) are solved for n^*, the result is

$$n^* = \frac{1+(1-\mathcal{T}^2)^{1/2}}{\mathcal{T}} \quad (\alpha = 0). \tag{32}$$

Implicit in the derivations given above is the assumption that n^* is independent of wavelength.[20] The determination of the dependence of n^* on wavelength requires reflectance spectra, which were not obtained for this study.

IV. RESULTS AND DISCUSSION

The physical and electrical characteristics determined for the samples used in this study at 300, 77, and 5 K are given in Table I. For all but the four lowest-composition samples of this study, the electron concentration was independent of temperature, indicating that these samples were degenerate at all temperatures. For each sample, the magnitude and temperature dependence of the electron mobility were compared with a theoretical analysis[21] of the electron mobility that calculates the scattering of electrons by longitudinal optical phonons, longitudinal and transverse acoustic phonons, charged and neutral defects, heavy holes, and the compositional disorder potential of the alloy. The electron mobility is dominated by longitudinal optical phonon scattering above 100 K and by ionized impurity scattering below 100 K. Analysis of the mobility data for temperatures < 10 K indicates that samples with $x > 0.3$ are compensated by shallow acceptor states, which can provide a mechanism for the absorption of radiation at energies just below the fundamental energy gap.

A. Infrared transmittance

The temperature dependence of the infrared transmittance spectra measured for four samples which have x values of 0.153, 0.253, 0.297, and 0.555 is shown in Figs. 2–5. The transmission edge moves to higher wave numbers with increasing x value, and in low-x alloys it is strongly dependent on temperature. Well-defined interference fringes were observed in most of the samples investigated, and at small wave numbers the infrared transmittance decreased as a consequence of the free electron absorption.

For all samples, the infrared transmission spectra show similar characteristics as the sample temperature is decreased from 300 to 5 K. At 300 K the transmission edge is broadened by (1) electron-phonon interactions, which enable transitions to occur at energies below the fundamental energy gap and (2) the thermal distribution of conduction electrons with energies $2k_BT$ above and below the Fermi energy. As the sample temperature is lowered, both the strength of the phonon-assisted transitions and the thermal distribution of electrons decrease, and the transmission edges become steeper, as observed in Figs. 2–5. As the temperature decreases, the conduction-electron degeneracy increases, and

TABLE I. Compositions and electrical characteristics of $Hg_{1-x}Cd_xSe$ samples.

Sample No. (ingot no.)	Mole fraction of CdSe, x	Electron concentration (300 K) (cm^{-3})	Electron mobility (300 K) (cm^2/Vs)	Electron concentration (77 K) (cm^{-3})	Electron mobility (77 K) (cm^2/Vs)
1 (16EC8)	0.153	5.37×10^{16}	6.3×10^{3}	2.94×10^{16}	1.14×10^{5}
5 (16EB12)	0.194	5.09×10^{16}	5.0×10^{3}	4.65×10^{16}	5.8×10^{4}
10 (16EA6)	0.228	4.18×10^{16}	4.1×10^{3}	3.75×10^{16}	2.8×10^{4}
2 (18LG)	0.253	3.91×10^{16}	3.3×10^{3}	3.2×10^{16}	2.57×10^{4}
3 (24AC13)	0.297	1.27×10^{16}	2.82×10^{3}	1.27×10^{16}	1.79×10^{4}
11 (28AT10)	0.354	8.62×10^{16}	2.16×10^{3}	8.62×10^{16}	8.35×10^{3}
6 (28ATE7)	0.412	5.2×10^{16}	1.9×10^{3}	5.2×10^{16}	6.9×10^{3}
7 (28ATE2)	0.470	3.65×10^{16}	1.3×10^{3}	3.65×10^{16}	3.4×10^{3}
4 (40EB2A)	0.555	5.2×10^{16}	1.1×10^{3}	5.2×10^{16}	3.1×10^{3}
8 (40EA5)	0.653	3.63×10^{16}	1.02×10^{3}	3.63×10^{16}	2.2×10^{3}
9 (40EA2)	0.684	2.76×10^{16}	7.63×10^{2}	2.80×10^{16}	2.13×10^{3}

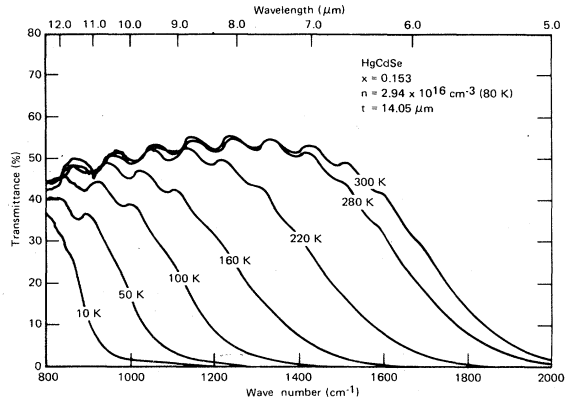

FIG. 2. Infrared transmittance spectra at different temperatures for $Hg_{0.847}Cd_{0.153}Se$ (sample 1).

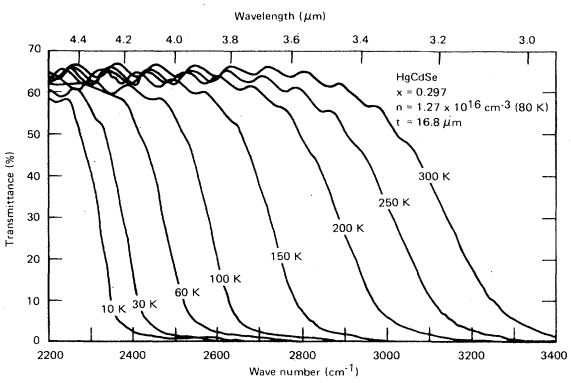

FIG. 4. Infrared transmittance spectra at different temperatures for $Hg_{0.703}Cd_{0.297}Se$ (sample 3).

as shown in Sec. IV C, the transmission edge more nearly corresponds to an apparent optical-energy gap equal to the Fermi energy E_F.

B. Refractive index

Figures 6 and 7 show the temperature and compositional dependences, respectively, of the refractive index of $Hg_{1-x}Cd_xSe$ alloys with $0.194 \leq x \leq 0.684$ between 5 and 300 K. These data were obtained from the spectral-transmission data using either Eq. (30) or (32). The refractive index depends strongly on crystal composition and temperature in low-x samples, and this dependence decreases rapidly with increasing x value. For example, for sample 5 with $x = 0.194$ (Fig. 6), the refractive index decreased by approximately 14% as the temperature was increased from 5 to 300 K, whereas for samples with x values greater than 0.55, the refractive index showed a small increase as the temperature was raised from 5 to 300 K. The compositional dependence of the refractive index, plotted in Fig. 7, decreases rapidly between x values of 0.15 and 0.4, and is small for higher x values. An extrapolation of the experimental refractive index values to $x = 1$ is in reasonable agreement with the average of the refractive index values reported by Verleur and Barker[22] for radiation polarized parallel and perpendicular to the c axis of CdSe.

At present it is not possible to quantitatively predict the temperature and compositional dependences of the refractive index for ternary semiconducting alloys. However, the observed behavior is consistent with the temperature and compositional dependences reported for the strong absorption edges associated with the zone center and X and L energy gaps,[23] which are related to the refractive index by the Kramers-Kronig relationship.

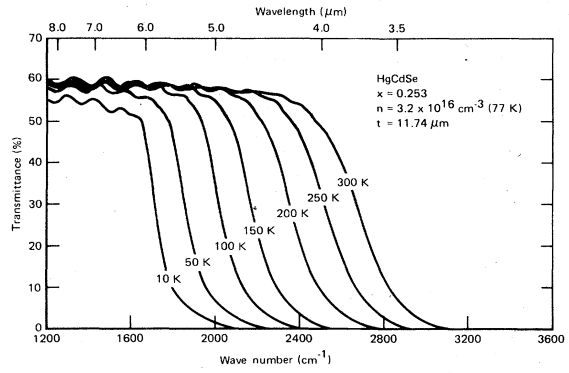

FIG. 3. Infrared transmittance spectra at different temperatures for $Hg_{0.747}Cd_{0.253}Se$ (sample 2).

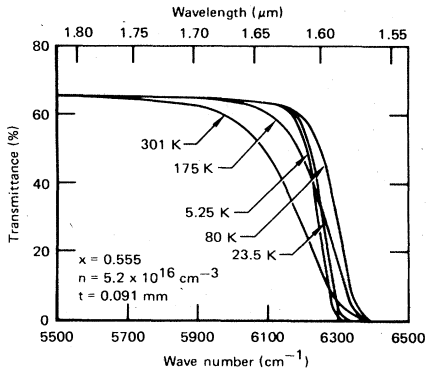

FIG. 5. Infrared transmittance spectra at different temperatures for $Hg_{0.445}Cd_{0.555}Se$ (sample 4). Well-defined interference fringes were observed in this sample but for clarity of presentation are not shown.

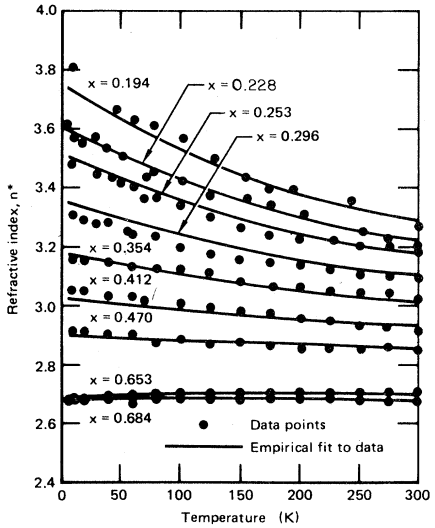

FIG. 6. Dependence of refractive index on temperature for $Hg_{1-x}Cd_xSe$ alloys with $0.194 < x < 0.684$.

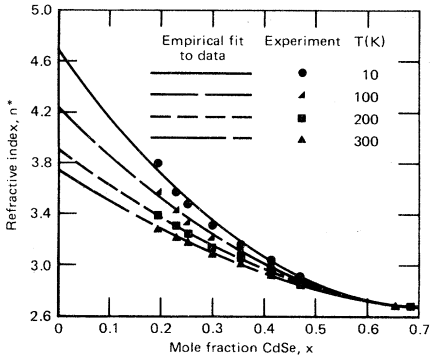

FIG. 7. Dependence of refractive index on crystal composition for temperatures of 10, 100, 200, and 300 K.

In $Hg_{1-x}Cd_xSe$ alloys with $x \leq 0.18$, which are either small-gap semiconductors or semimetals, some dependence of the refractive index on electron concentration is expected. This dependence arises because the strength of direct transitions between the valence band and conduction band near $k=0$ makes a large, frequency-dependent contribution to the dielectric constant in small band-gap semiconductors and is strongly affected by the electron distribution. This effect has been observed in narrow-band-gap $Hg_{1-x}Cd_xTe$ alloys[24] and is believed to be the cause of the dependence of the high-frequency dielectric constant on electron concentration observed in HgSe by Manabe and Mitsuishi.[25] Because of this effect, data from samples with x values less than 0.19 were omitted from a least-squares fit to obtain the compositional dependence of the refractive index, as were data from sample 4 which showed anomalously high values for n^*.

The compositional and temperature dependences of the refractive index are given by the following empirical expression:

$$n^* = 4.729(1 - 1.237x + 0.883x^2) - 5.679\times10^{-3}(1 - 3.355x + 2.724x^2)T + 7.717\times10^{-6}(1 - 3.443x + 2.781x^2)T^2, \quad (33)$$

where the values for the coefficients were obtained from a least-squares analysis of all the data acquired for the $Hg_{1-x}Cd_xSe$ alloy system. The empirical fit given by Eq. (33) describes the experimentally determined values of the refractive index to an accuracy of ±2% for the range of alloy compositions and temperatures measured and is compared with the experimental data in Figs. 6 and 7.

C. Analysis of absorption spectra

The absorption spectra were analyzed to obtain the energy gap E_G and Fermi energy E_F as functions of composition and temperature for the $Hg_{1-x}Cd_xSe$ alloys by fitting the theoretical expressions derived in Sec. II to the experimental data. Values for E_G, P, and $\tau_{c,hh}$ were obtained by treating these quantities as variables in a least-squares fitting routine which minimized the rms deviation between the theoretical and experimental absorption curves. Because the computation time for this procedure would have been excessive if all the data points were used, the theoretical curve was fitted to representative values of the absorption coefficient selected at energy values that fully described the curvature of the absorption spectrum. To minimize possible errors from contributions to the absorption spectrum from near-band-gap acceptor-state to conduction-band transitions, valence-band to donor-state transitions, and band tailing, experimental absorption coefficient values greater than 80 cm^{-1} were selected for this fitting procedure.

In the fitting procedure, the refractive-index values obtained in this work were used. A value of 0.45 eV was used for Δ because this value gives a good fit to Shubnikov–de Haas data for HgSe (Ref. 26) and low-x $Hg_{1-x}Cd_xSe$ alloys.[8] A value of 0.43 has been reported for Δ in CdSe (Ref. 5). No data exist for determining the values of μ_{hh} in $Hg_{1-x}Cd_xSe$ alloys, and the value used, $\mu_{hh} = 0.50\, m_0$, is an approximation based on the band parameters of other semiconductors. A

value of 5×10^{-12} s was used for the electron and hole mean free times τ_c and τ_{hh}.

Calculations were made to determine the effect of the values used for Δ, μ_{hh}, and τ_c and τ_{hh} on the least-squares determinations of E_G, P, and $\tau_{c,hh}$, which was assumed equal to $\tau_{c,lh}$. The values used for the spin-orbit coupling and heavy-hole mass were varied by $\pm10\%$, and τ_c and τ_{hh} were varied by an order of magnitude. The experimental absorption data were then refitted to obtain new values for E_G, P, and $\tau_{c,hh}$. For sample 6 ($x=0.412$) at 250 K, variations of Δ and μ_{hh} changed E_G, P, and $\tau_{c,hh}$ be less than $\pm0.1\%$, $\pm3\%$, and $\pm6\%$, respectively. The variations of τ_c or τ_{hh} changed E_G, P, and $\tau_{c,hh}$ by less than 0.05%, 0.5%, and 2%, respectively. Similar fits to the spectrum of sample 6 at 10 K showed that E_G, P, and $\tau_{c,hh}$ changed by approximately half the above values. The same procedure was also performed on the smallest band-gap sample 1 ($x=0.153$). At 250 K similar results were obtained, the variations in E_G, P, and $\tau_{c,hh}$ being approximately 50% larger than those given for sample 6 at 250 K. For the low-temperature <40 K data recorded on sample 1, larger changes for E_G, P, and $\tau_{c,hh}$ were observed. The variations of μ_{hh}, τ_c, and τ_{hh} resulted in changes of $\pm1\%$, $\pm1\%$, and $\pm20\%$ in E_G, P, and $\tau_{c,hh}$, respectively, and the variations of Δ produced changes of less than $\pm4\%$, $\pm3\%$, and $\pm30\%$ for E_G, P, and $\tau_{c,hh}$, respectively. Thus, except for alloy compositions with band gaps <0.1 eV, errors in the values used for Δ, μ_{hh}, τ_c, or τ_{hh} produced insignificant errors in the determinations of E_G and P and only a small error in $\tau_{c,hh}$. Representative examples of the data fitting obtained for low- and high-x $Hg_{1-x}Cd_xSe$ compositions are shown in Figs. 8 and 9 for samples 2 and 4, respectively. The experimental values plotted for the absorption coefficients in Figs. 8 and 9 were calculated from the transmittance data by using Eq. (28) and the values measured for n^*.

For sample 2 at 30 K, the best fit [Fig. 8(a)] was obtained with $E_G=0.200$ eV, $P=7.91\times10^{-8}$ eV cm, $E_F=0.221$ eV, and $\tau_{c,hh}=\tau_{c,lh}=3.79\times10^{-12}$ s. The values obtained for E_G is significantly less than the energy at which the absorption coefficient becomes appreciable. This difference occurs because the sample is degenerate at 30 K and the Fermi energy lies in the conduction band; thus E_F is the minimum energy for which optical transitions are possible.

At 125 K [Fig. 8(b)], the best fit to the data for sample 2 is obtained with $E_G=0.249$ eV and $P=8.01\times10^{-8}$ eV cm. At this higher temperature, E_F has decreased to 0.261 eV, 0.011 eV above the conduction-band minimum, but the electron

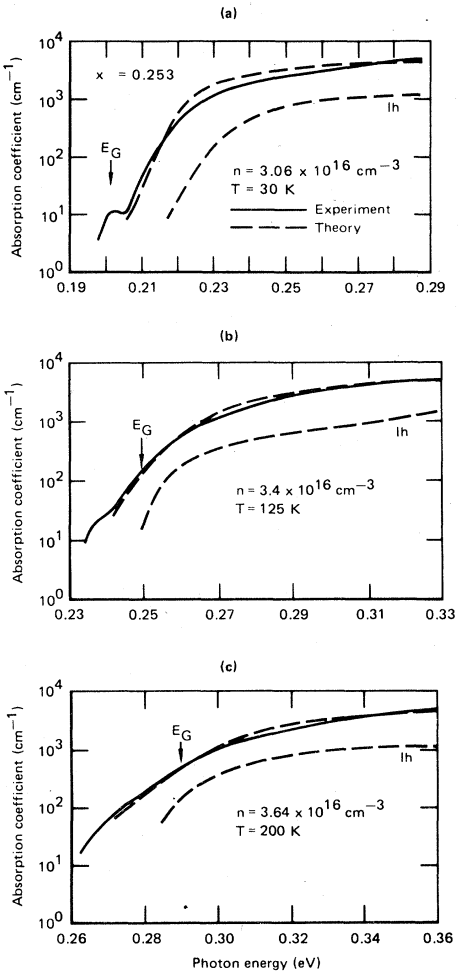

FIG. 8. Theoretical and experimental absorption coefficient spectra for sample 2 ($x=0.253$) at (a) 30 K, (b) 125 K, and (c) 200 K.

concentration is distributed over an appreciable energy range about E_F. This range is approximately $4k_BT$, and thus if there are vacant states within $2k_BT$ (0.021 eV) of E_F, electrons can be optically excited into these states from the valence band. For these conditions, therefore, the onset of optical absorption occurs near E_G, as observed. The change in the shape of the absorption edge as the sample temperature increases from 30 to 125 K was greater than could be explained by considering only the effect of the increased thermal distribution of electrons in the conduction band. To obtain the fit for 2 shown in Fig. 8(b), the value used for $\tau_{c,hh}$ (and $\tau_{c,lh}$) is 1.91×10^{-12} s, which is half the value used at 30 K. The effect of decreasing $\tau_{c,hh}$ and $\tau_{c,lh}$ is to broaden the linewidth of each optical transition across

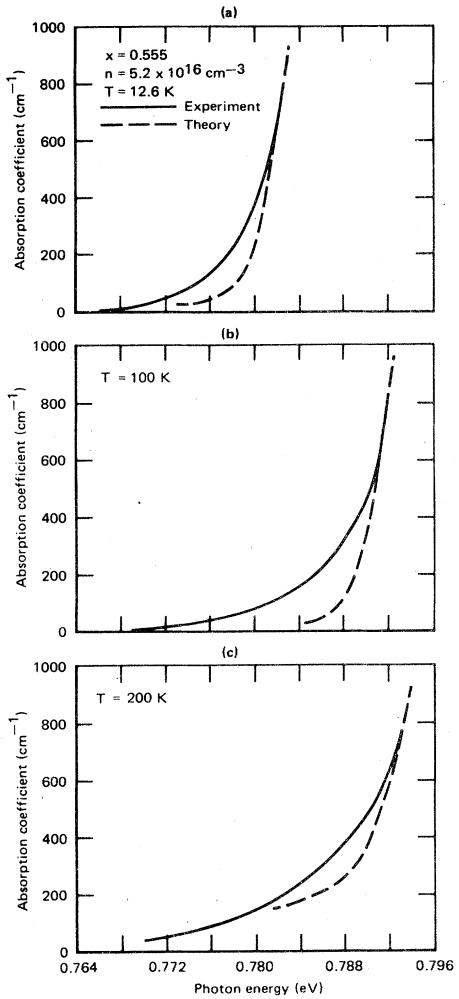

FIG. 9. Theoretical and experimental absorption coefficient spectra for sample 4 at (a) 12.6 K, (b) 100 K, and (c) 200 K.

the energy gap and thus to reduce the slope of the absorption edge by allowing optical transitions to occur at photon energies less than E_G. These effects are even more apparent in sample 2 at 200 K [Fig. 8(c)] where values of $E_G = 0.289$ eV, $P = 8.06 \times 10^{-8}$ eV cm, and $\tau_{c,hh} = \tau_{c,lh} = 4.58 \times 10^{-13}$ s were required to fit the data.

The theoretically calculated contribution to the absorption coefficient from transitions between the light-hole valence band and conduction band is also shown in Fig. 8. The onset of these transitions occurs at an energy E_F-E_G, above the heavy-hole valence-band-to-conduction-band transition energy because of the similar dependences of E on k for the conduction and light-hole valence bands in the Kane model. At higher energies it was found that direct optical transitions originating from the light-hole band contribute approximately 35% of the magnitude of the total absorption coefficient.

Because of the difficulty in preparing $Hg_{1-x}Cd_xSe$ alloys with high x values, fewer samples with $x \geq 0.5$ were prepared and therefore thinned to only 80–100 μm to minimize sample losses. This limited the absorption coefficient values that could be measured to < 1000 cm^{-1} and thus reduced the effectiveness of the least-squares analyses. For samples with $x > 0.45$, the absorption edge was considerably broader than measured in low-x samples, and in some high-x samples a long tail was observed below the absorption edge which was attributed to compensation. For some samples with $x > 0.45$, it was difficult to consistently obtain a unique fit to the data using physically realistic band parameters unless the momentum matrix element was kept constant at a value of 8.0×10^{-8} eV cm. This P value gave the best fit to the optical absorption spectra for low x-value samples and is in excellent agreement with the values obtained by Stankiewicz *et al.*[8] from Shubnikov–de Haas studies on $Hg_{1-x}Cd_xSe$ samples with $x < 0.19$. The effect of this restriction of P on the computed values obtain for E_G was small, $\leq 3\%$.

Fits of the theoretical expression to the absorption spectra for sample 4 at 12.6, 100, and 200 K are demonstrated in Fig. 9. The fit at 12.6 K [Fig. 9(a)] was obtained with $E_G = 0.7725$ eV and E_F-$E_G = 0.0094$ eV. Even for this wide-gap alloy, the value obtained for E_G is significantly below the energy at which the absorption coefficient becomes appreciable because of the sample degeneracy for this temperature and electron concentration.

At 100 K, the best fit to the data was obtained with $E_G = 0.7895$ eV. At this higher temperature, E_F-E_G has decreased to 0.00087 eV, and E_F is effectively coincident with the bottom of the conduction band. However, because of the higher temperature, the electron concentration is distributed over an appreciable energy range (± 0.017 eV) about E_F. States 0.017 eV above E_F are partially filled, and therefore the rate of optical transitions into these levels is reduced. Similarly, energy levels within 0.017 eV below E_F have vacant states into which electrons can be optically excited from the valence band.

Figure 9(c) shows the best fit that can be obtained for 4 at 200 K. The theoretical curve is for $E_G = 0.7915$ eV, and the computed value for the Fermi energy is 0.0214 eV below the conduction-band minimum. The tail of the absorption edge at energies below E_G, which is most pronounced at sample temperatures of 100 and 200 K, is attributed either to phonon-assisted transitions,

which enable optical absorption to occur at energies less than E_G, or to the presence of many shallow-donor states that overlap the conduction band and provide a continuum of energy levels below the conduction-band minimum. Only at higher temperatures, for which the Fermi energy is near or below the bottom of the conduction band, can such states be partially ionized and therefore available for optical transitions at photon energies less than E_G.

D. Dependence of energy gap on temperature and composition

From a series of analyses similar to those described in the last section, the dependence of E_G, E_F, P, and $\tau_{c,hh}$ on temperature was obtained for each sample. The temperature dependences of E_G and E_F are depicted in Figs. 10 and 11 for samples 1 ($x=0.153$) and 4 ($x=0.555$), respectively. Figure 10 shows the strong linear dependence of E_G on temperature that was observed in all low-x samples. In sample 1, for example, the energy gap increased more than 300%, from 0.064 to 0.213 eV, as the temperature increased from 5 to 300 K. The values computed from the theoretical analysis also confirm that the sample is degenerate below 270 K and explain the large Moss-Burstein shift of the absorption edge to higher energies as observed in Fig. 8. The magnitude of this shift increases with decreasing temperature, and at 5 K the apparent optical-absorption gap is ≈ 0.105 eV, 65% larger than the fundamental energy gap of 0.0640 eV. Because the electron concentration of this sample was nearly independent of temperature, the increase of E_F-E_G with decreasing temperature is a direct measure of the dependence of the conduction-band curvature on the energy gap. Figure 10 clearly demonstrates the gross errors that can result in measuring energy gaps and their temperature dependence in narrow-band-gap semiconductors unless the data are analyzed to correctly consider the electron concentration and its temperature dependence. Similar effects, but of progressively decreasing magnitude with increasing x values, were observed in all samples.

For samples with x values greater than 0.45, the energy gap does not increase linearly with temperature between 5–300 K. Sample 7 ($x=0.47$) displayed a small sublinear dependence of the energy gap on temperature between 5 and 300 K, and a more complicated behavior was observed in samples 4, 8, and 9. Below 70 K the energy gap of high-x samples increases with temperature, but at a rate that decreases with increasing sample composition. Above 70 K the temperature dependence of the energy gap changes more rapidly with increasing x value, and for samples with $x>0.555$ the energy-gap temperature coefficient is negative. This effect is demonstrated by Fig. 11, where the energy gap of sample 4 increases between 5 and 70 K but is nearly independent of temperature above 100 K. For samples 8 and 9, the energy gap decreases with increasing temperature above 70 K. This behavior is in agreement with the results plotted in Fig. 12, where the average temperature coefficient of the energy gap is plotted as a function of sample composition. The dependence of the energy-gap temperature coefficient on crystal

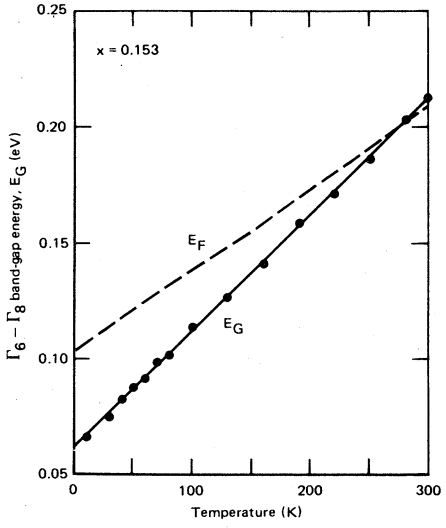

FIG. 10. Dependence of the fundamental direct energy gap and the Fermi energy temperature for sample 1, $x=0.153$.

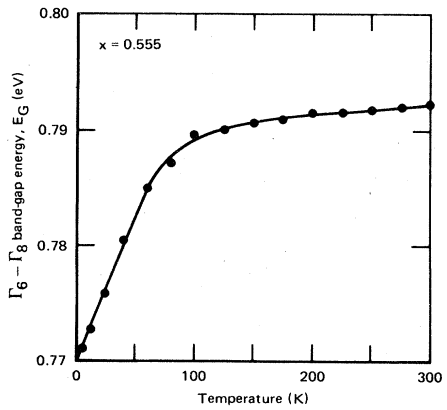

FIG. 11. Dependence of the fundamental energy gap on temperature for sample 4, $x=0.555$.

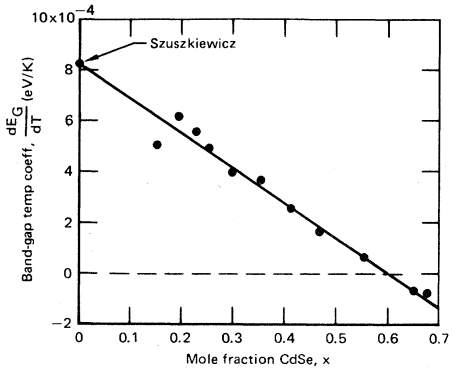

FIG. 12. Compositional dependence of the temperature coeffieient of the fundamental direct energy gap on alloy composition for $Hg_{1-x}Cd_xSe$ alloys with $0.153 < x < 0.684$.

composition shows that alloys with $x > 0.60$ have negative temperature coefficients between 5–300 K. The least-squares fit to the data plotted in Fig. 12 is in excellent agreement with the value of the energy-gap temperature coefficient obtained for HgSe by Szuszkiewicz.[27]

To obtain a functional relationship for the dependence of the energy gap in $Hg_{1-x}Cd_xSe$ alloys on crystal composition and temperature, all the data accumulated in this investigation were least-squares analyzed with an expression of the form of Eq. (33) in which the energy gap is expressed to second order in alloy composition and temperature:

$$E_G = -0.209(1 - 7.172x - 2.174x^2) + 7.37\times10^{-4}(1 - 1.277x - 0.151x^2)T + 2.001\times10^{-9}(1 + 23.45x - 599.4x^2)T^2, \quad (34)$$

where E_G is in eV, T is in K, and x is the mole fraction of CdSe in the alloy.

The experimental data and fit given by Eq. (34) are compared in Figs. 13 and 14 as functions of temperature and crystal composition, respectively. As shown in Fig. 14, a good fit is obtained to the data for all but the lowest x value, and a higher-order polynomial, as has been used for HgCdTe alloys,[28] possibly would more accurately express the compositional dependence of E_G on temperature. However, the discrepancy at low x value probably results because the Kane model used in this work does not adequately describe the conduction-band curvature for energies $\gg E_G$ in semiconductors with $E_G \leq 0.1$ eV. Figure 14 clearly demonstrates that at all temperatures the energy gap of $Hg_{1-x}Cd_xSe$ alloys bows below a linear interpolation between the energy gaps of HgSe and CdSe.

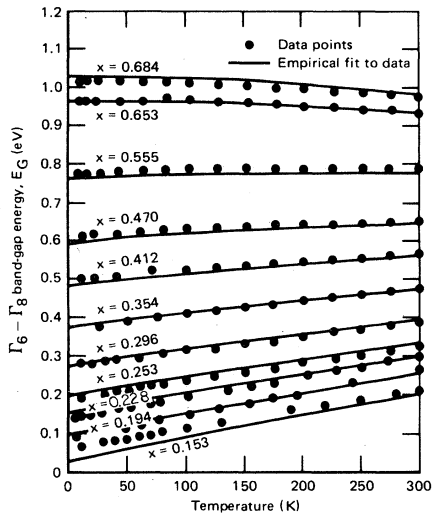

FIG. 13. Dependence of the fundamental direct energy gap of $Hg_{1-x}Cd_xSe$ alloys on temperature for measured alloy compositions.

For the theoretical fits made to the absorption spectra for samples with $x < 0.45$, a value for P of $8.0 \pm 0.2 \times 10^{-8}$ eV cm was obtained and showed no discernable dependence on sample composition or temperature.

The values of the lifetimes of the conduction-band-to-heavy-hole and conduction-band-to-light-hole transitions that gave the best fit to the absorption spectra are plotted in Fig. 15 as functions of temperature for alloy compositions between $x = 0.153$ and 0.47. The lifetimes for samples with $x \leq 0.354$ show little temperature dependence below 50 K, but between 50 and 300 K the lifetimes decrease exponentially with temperature

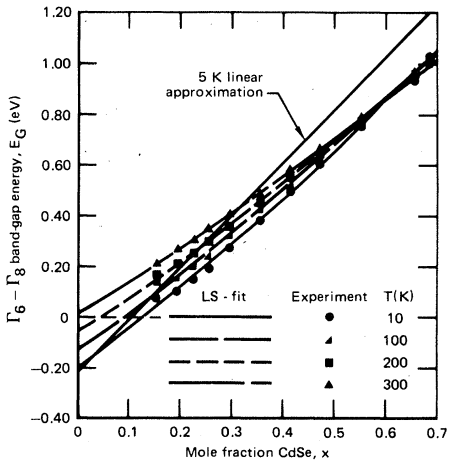

FIG. 14. Dependence of the fundamental direct energy gap of $Hg_{1-x}Cd_xSe$ alloys on crystal composition for temperatures of 10, 100, 200, and 300 K.

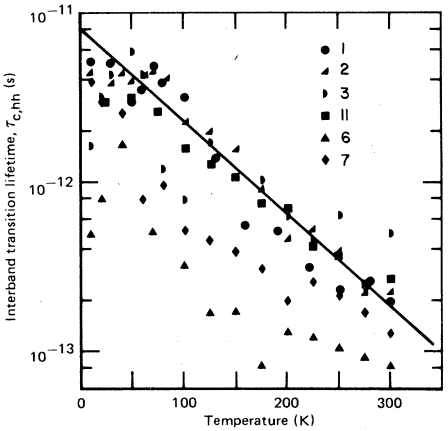

FIG. 15. Dependence of direct band gap transition lifetimes on temperature for $Hg_{1-x}Cd_xSe$ alloys with $0.153 < x < 0.470$.

from 5×10^{-12} to 2×10^{-13} s. The temperature dependence in this region obeys the relationship $\tau_{c,hh}(T) = \tau_{c,hh}(0)\exp(-AT)$, which is plotted as a solid line in Fig. 15 for values of $\tau_{c,hh}(0) = 8\times10^{-12}$ s and $A = 2.01\times10^{-2}$ K^{-1}. The lifetimes obtained for samples with x values greater than 0.354 have similar temperature dependences but are from 2 to 5 times shorter than the values obtained in lower-x samples and show considerably more scatter.

The analysis can be further refined by the inclusion of higher-band terms, alloy-disorder terms, and by the formulation of a temperature-dependent Kane band theory. In the former case, any correction is expected to be small because Shubnikov–de Haas data show that for samples with electron concentrations below 1×10^{17} cm^{-3}, the effect of higher-band terms on the conduction-band curvature is small.[8] The relatively small departure of the compositional dependence of E_G from a linear interpolation between the energy gaps of HgSe and CdSe suggests that for the $Hg_{1-x}Cd_xSe$ alloy system, the effect of alloy disorder on the conduction-band shape is small. Results of this investigation show that for samples with different energy-gap temperature coefficients, i.e., 1 ($x=0.153$) and 7 ($x=0.47$), good fits are obtained to the data and consistent trends are observed in the temperature and compositional dependences of band parameters used to obtain these fits. These results suggest that for the HgCdSe alloy system, a temperature-dependence energy gap should be used in the Kane model. However, to confirm the above conclusion requires further measurements on samples of constant composition spanning a range of electron concentrations. The temperature dependence of the conduction-band curvature could then be obtained from the measured dependence of the Fermi energy on electron concentration and temperature. In addition to an experimental confirmation of the above conclusions, a comprehensive theory of the temperature dependence of the band parameters is required for improving band-structure calculations and obtaining fits to experimental data.

At present, two theoretical approaches have been developed to explain the observed dependence of the energy gap on crystal composition in ternary semiconductors. Hill[29] has argued that the virtual crystal approximation (VCA), in which the randomly varying crystal potential in an alloy is approximated by a periodic lattice of average atomic potentials, is sufficient to calculate the band structure of alloys. However, other investigators[11,14,30-32] find that the VCA approximation predicts a smaller bowing of the energy gap than observed experimentally and claim that the inclusion of disorder effects improves the agreement between theory and experiment. Methods used to calculate the magnitude of the disorder potential range from the semiempirical dielectric model first proposed by Van Vechten and Bergstresser[11] to various VCA-based perturbation approaches developed by Stroud,[30] Siggia,[14] Baldereshi and Manshke,[31] and Schulze, Newman, and Unger.[32] Unfortunately, direct comparison between these methods are obscured by different alloy investigations and by the use of different sets of potential form factors which have a critical effect on the results of the calculations.

The temperature dependence of the energy-band gap in solids arises because the lattice vibrations of the crystal produce a temperature-dependent electronic band structure. An exact calculation of the temperature dependence of the energy gap should include the contributions from thermal expansion, Debye-Waller scattering,[33] and the Fan[34] intra- and inter-band transition terms. Because many of the material constants required to calculate the magnitude of these contributions are not known for the $Hg_{1-x}Cd_xSe$ alloy system, no attempt was made to analyze the temperature dependences of the energy-gap values measured in this investigation.

To avoid some of the complexity of the quantum-mechanical calculations mentioned, Heine and Van Vechten[35] formulated a thermodynamic treatment of the temperature dependence of the energy gap and obtained a good fit to the data for Si. Their model provides physical insight into the mechanism responsible for the positive energy-gap temperature coefficient in HgTe, HgSe, and

low-x $Hg_{1-x}Cd_xTe$ and $Hg_{1-x}Cd_xSe$ alloys, but to obtain quantitative agreement between experiment and theory requires detailed knowledge of the magnitude of the mixing of the symmetry character of the wave functions at the edges of the valence and conduction bands. The magnitude of the mixing is related to the magnitude of the alloy-disorder potential. Camassel and Auvergne[36] have shown that slightly different sets of band-structure parameters can give nearly identical band shapes near $k=0$, but produce different values for the temperature coefficient of the fundamental energy gap. Thus, it appears that the most accurate values for the fundamental band-structure constants and pseudopotentials will be obtained from simultaneous fits of theoretically predicted band gaps to experimental determinations of the compositional and temperature dependences of these quantities as reported herein.

Another manifestation of the strong electron-phonon coupling present in this alloy system is the observed decrease in band-to-band transition lifetimes with increasing temperature. From the uncertainty principle, the decrease in transition lifetime can be related directly to an increase in the width of conduction-band levels into which electrons can be photon excited. The physical mechanism for this broadening is associated with the thermal displacement of ions from their equilibrium lattice sites and results in a progressive coupling of neighboring electronic energy levels with increasing temperature. Thus a relationship between the lifetimes and the Debye-Waller scattering term is expected.

V. CONCLUSIONS

This paper summarizes results of a comprehensive investigation of the optical properties of zinc-blende $Hg_{1-x}Cd_xSe$ alloys with $0.15 \leq x \leq 0.68$. Empirical relationships have been obtained which describe the dependence of the refractive index and energy gap on composition and temperature to an accuracy of better than $\pm 2\%$. It has been shown that the energy gap is not linear in x over the range $0 \leq x \leq 0.68$ and can lie as much as 0.16 eV below the linear interpolation between the energy gaps of HgSe and wurtzite CdSe. For samples with x values less than 0.45, the energy gap increases linearly with temperature from 5–300 K, but shows marked deviations from this behavior in higher-x samples. The origin of the large, positive, energy-gap temperature coefficient in the low-x alloys is unexplained and requires further theoretical work.[37]

ACKNOWLEDGMENTS

The authors are indebted to D. A. Nelson, who grew the single crystals and performed many of the sample characterizations for this study. The technical assistance of Mr. D. S. Wright and Mr. J. D. Putnam is gratefully acknowledged. This research was supported by Office of Naval Research Contract No. N00014-74-C-0318, Air Force Materials Labortory Director's Funds Contract No. F33615-74-C-5167, and by the McDonnell-Douglas Corporation Independent Research and Development program.

APPENDIX A

The functions appearing in the transition matrix elements of Eqs. (7) and (8) are defined as follows:

$$\begin{aligned} L_2^{lh\text{-}c} = {} & 2a_{lh}^2(a_c A_{2c} + 2kA_{1c}^2) + 2b_{lh}^2(b_c B_{2c} + 2kB_{1c}^2) + 2c_{lh}^2(c_c C_{2c} + 2kC_{1c}^2) \\ & + 2a_{lh}[a_c(b_{lh}B_{2c} + c_{lh}C_{2c}) + A_{2c}(b_{lh}b_c + c_{lh}c_c) + 4kA_{1c}(b_{lh}B_{1c} + c_{lh}c_{1c})] \\ & + 2b_{lh}c_{lh}(b_c c_{2c} + c_c B_{2c} + 4kB_{1c}C_{1c}) . \end{aligned} \tag{A1}$$

$$\begin{aligned} L_0^{lh\text{-}c} = {} & \tfrac{1}{2}[2(a_{lh}a_c)(b_{lh}b_c + c_{lh}c_c) + \tfrac{3}{2}(b_{lh}b_c)^2 + \sqrt{2}\,(b_{lh}b_c)(b_{lh}c_c + c_{lh}b_c) \\ & + 4(b_{lh}c_c)(c_{lh}c_c) - (b_{lh}c_c + c_{lh}b_c)^2 + 2(c_{lh}c_c)^2] , \end{aligned} \tag{A2}$$

$$a_c = \frac{[E_c(E_c+\Delta)(E_c+2\Delta/3)]^{1/2}}{N_c} , \tag{A3}$$

$$b_c = \frac{\sqrt{2}\,\Delta(E_c - E_G)^{1/2}}{3N_c} , \tag{A4}$$

$$c_c = \frac{(E_c - E_G)^{1/2}(E_c + 2\Delta/3)}{N_c} , \tag{A5}$$

$$N_c=[E_c(E_c+\Delta)(E_c+2\Delta/3)+\frac{2\Delta^2}{9}(E_c-E_G)+(E_c-E_G)(E_c+2\Delta/3)^2]^{1/2}, \tag{A6}$$

$$\{A_{1c}, B_{1c}, C_{1c}\}=k\frac{d}{d(k^2)}\{a_c, b_c, c_c\}, \tag{A7}$$

$$\{A_{2c}, B_{2c}, C_{2c}\}=2k^3\frac{d^2}{d(k^2)^2}\{a_c, b_c, c_c\}, \tag{A8}$$

$$a_{lh}=\frac{[-E_{lh}(E_{lh}+\Delta)(E_{lh}+2\Delta/3)]^{1/2}}{N_{lh}}, \tag{A9}$$

$$b_{lh}=\frac{-\sqrt{2}\,\Delta}{3}\frac{(E_G-E_{lh})^{1/2}}{N_{lh}}, \tag{A10}$$

$$c_{lh}=\frac{-(E_G-E_{lh})^{1/2}(E_{lh}+2\Delta/3)}{N_{lh}}, \tag{A11}$$

and

$$N_{lh}=[-E_{lh}(E_{lh}+\Delta)(E_{lh}+2\Delta/3)+\tfrac{2}{9}\Delta^2(E_G-E_{lh})+(E_G-E_{lh})(E_{lh}+2\Delta/3)^2]^{1/2}. \tag{A12}$$

[1]D. A. Nelson, C. J. Summers, and C. R. Whitsett, J. Electron Mater. 6, 507 (1977).
[2]S. Groves and W. Paul, in *Physics of Semiconductors, Proceedings of the 7th International Conference*, edited by M. Hulin (Dunod, Paris, 1964), p. 41.
[3]C. R. Whitsett, Phys. Rev. 138, A829 (1965).
[4]S. L. Lehoczky, J. G. Broerman, D. A. Nelson, and C. R. Whitsett, Phys. Rev. B 9, 1598 (1974).
[5]R. G. Weeler and J. O. Dimmock, Phys. Rev. 125, 1805 (1962).
[6]C. Konák, J. Dillinger, and V. Prosser, in *II-VI Semiconducting Compounds*, edited by D. G. Thomas (Benjamin, New York, 1967), p. 850.
[7]A. Kalb and V. Leute, Phys. Status Solidi 5, K199 (1971).
[8]J. Stankiewicz, W. Giriat, and W. Dorbrowolski, Phys. Status Solidi B 61, 267 (1974).
[9]P. S. Kireev and V. V. Volkov, Fiz. Tekh. Poluprovodn. 7, 1419 (1973) [Sov. Phys. Semicond. 7, 949 (1974)].
[10]P. A. Slodowy and W. Giriat, Phys. Status Solidi B 48, 463 (1971).
[11]J. A. Van Vechten and T. K. Bergstresser, Phys. Rev. B 1, 3351 (1970).
[12]E. O. Kane, J. Phys. Chem. Solids 1, 249 (1957).
[13]O. Berolo, J. C. Woolley, and J. A. Van Vechten, Phys. Rev. B 8, 3794 (1973).
[14]E. D. Siggia, Phys. Rev. B 10, 5147 (1974).
[15]H. Ehrenreich, J. Phys. Chem. Solids 2, 131 (1957).
[16]J. G. Broerman, in *Physics of Semiconductors; Proceedings of the Eleventh International Conference* (Polish Scientific, Warsaw, 1972), p. 417.
[17]H. A. Bowman and R. M. Schooner, J. Res. Natl. Bur. Stand. 71C, 179 (1967).
[18]L. J. van der Pauw, Philips Res. Rep. 13, 1 (1958).
[19]M. P. Lisita, V. N. Malinko, E. V. Pidlisnyi, and G. G. Tsebulya, Surf. Sci. 11, 411 (1968).
[20]T. S. Moss, *Optical Properties of Semiconductors* (Butterworths, London, 1959), p. 12.
[21]D. A. Nelson, J. G. Broerman, C. J. Summers, and C. R. Whitsett, Phys. Rev. B 18, 1658 (1978).
[22]H. W. Verleur and A. S. Barker, Jr., Phys. Rev. 155, 750 (1967).
[23]I. N. Borisov, P. S. Kireev, V. V. Makhailin, and V. M. Bezborodova, Fiz. Tekh. Poluprovodn. 5, 829 (1971) [Sov. Phys. Semicond. 5, 734 (1971)].
[24]A. Polian, R. Letoullec, and M. Balkanski, Phys. Rev. B 13, 3558 (1976).
[25]A. Manabe and A. Mitsuishi, Solid State Commun. 16, 743 (1975).
[26]D. G. Seiler, R. R. Galazka, and W. M. Becker, Phys. Rev. 133, 4274 (1971).
[27]W. Szuszkiewicz, in *Proceedings of the Third International Conference on the Physics of Narrow Gap Semiconductors*, edited by J. Rauluszkiewicz, M. Górska, and E. Kaczmarek (Polish Scientific, Warsaw, 1978), p. 93.
[28]J. L. Schmit and E. L. Stelzer, J. Appl. Phys. 40, 4865 (1969).
[29]R. Hill, J. Phys. C 7, 521 (1973).
[30]D. Stroud, Phys. Rev. B 5, 3366 (1972).
[31]A. Baldereshi and K. Maschke, Solid State Commun. 16, 99 (1975).
[32]K. R. Schulze, N. Newman, and K. Unger, Phys. Status Solidi B 75, 493 (1976).
[33]C. Keffer, T. M. Hayes, and A. Bienenstock, Phys. Rev. Letters 21, 1676 (1968).
[34]H. Y. Fan, Phys. Rev. 82, 900 (1954).
[35]V. Heine and J. A. Van Vechten, Phys. Rev. B 13, 1622 (1976).
[36]J. Camassel and D. Auvergne, Phys. Rev. B 12, 3258 (1975).
[37]C. S. Guenzer and A. Bienenstock, Phys. Rev. B 8, 4655 (1973).